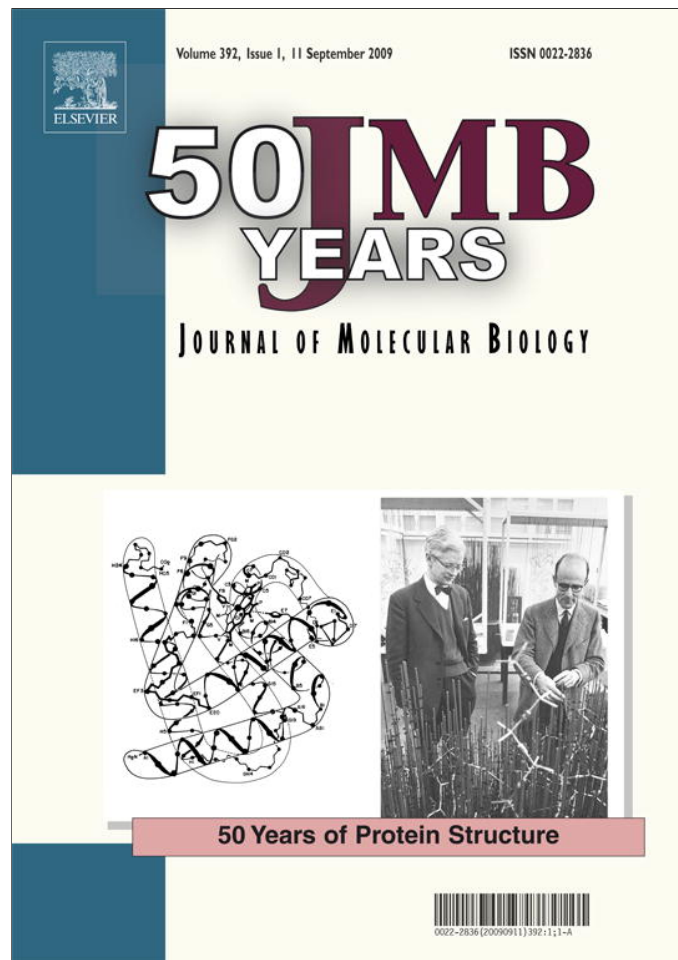


Provided for non-commercial research and education use.
Not for reproduction, distribution or commercial use.



This article appeared in a journal published by Elsevier. The attached copy is furnished to the author for internal non-commercial research and education use, including for instruction at the authors institution and sharing with colleagues.

Other uses, including reproduction and distribution, or selling or licensing copies, or posting to personal, institutional or third party websites are prohibited.

In most cases authors are permitted to post their version of the article (e.g. in Word or Tex form) to their personal website or institutional repository. Authors requiring further information regarding Elsevier's archiving and manuscript policies are encouraged to visit:

<http://www.elsevier.com/copyright>

JMBAvailable online at www.sciencedirect.com

ScienceDirect


Crystal Structure of Miner1: The Redox-active 2Fe-2S Protein Causative in Wolfram Syndrome 2

Andrea R. Conlan¹, Herbert L. Axelrod², Aina E. Cohen²,
Edward C. Abresch³, John Zuris¹, David Yee³, Rachel Nechushtai⁴,
Patricia A. Jennings^{1*} and Mark L. Paddock^{3*}

¹Departments of Chemistry and Biochemistry, University of California at San Diego, La Jolla, CA 92093, USA

²Stanford Synchrotron Radiation Lightsource, 2575 Sand Hill Road, Menlo Park, CA 94025, USA

³Department of Physics, University of California at San Diego, La Jolla, CA 92093, USA

⁴Department of Plant and Environmental Sciences, The Wolfson Centre for Applied Structural Biology, Hebrew University of Jerusalem, Givat Ram 91904, Israel

Received 5 May 2009;
received in revised form
26 June 2009;
accepted 29 June 2009
Available online
4 July 2009

Edited by M. Guss

The endoplasmic reticulum protein Miner1 is essential for health and longevity. Mis-splicing of CISD2, which codes for Miner1, is causative in Wolfram Syndrome 2 (WFS2) resulting in early onset optic atrophy, diabetes mellitus, deafness and decreased lifespan. In knock-out studies, disruption of CISD2 leads to accelerated aging, blindness and muscle atrophy. In this work, we characterized the soluble region of human Miner1 and solved its crystal structure to a resolution of 2.1 Å (*R*-factor=17%). Although originally annotated as a zinc finger, we show that Miner1 is a homodimer harboring two redox-active 2Fe-2S clusters, indicating for the first time an association of a redox-active FeS protein with WFS2. Each 2Fe-2S cluster is bound by a rare Cys₃-His motif within a 17 amino acid segment. Miner1 is the first functionally different protein that shares the NEET fold with its recently identified paralog mitoNEET, an outer mitochondrial membrane protein. We report the first measurement of the redox potentials (*E*_m) of Miner1 and mitoNEET, showing that they are proton-coupled with *E*_m ~0 mV at pH 7.5. Changes in the pH sensitivity of their cluster stabilities are attributed to significant differences in the electrostatic distribution and surfaces between the two proteins. The structural and biophysical results are discussed in relation to possible roles of Miner1 in cellular Fe-S management and redox reactions.

Published by Elsevier Ltd.

Keywords: diabetes; membrane bound; oxidative stress; CDGSH; ER stress

Introduction

Miner1[†], originally annotated as a zinc finger protein of unknown function, is actually a unique redox-active Fe-S protein. The gene encoding Miner1, CISD2 (CDGSH iron sulfur domain 2[‡]),

found at chromosomal location 4q24, was identified recently as the carrier of a mutation that causes Wolfram Syndrome 2 (WFS2).¹ The pre-mRNA of CISD2 has two splice sites, creating three exons and two introns (Fig. 1). Correct splicing is essential for the proper translation and function of Miner1. It localizes to the endoplasmic reticulum (ER) when properly expressed and folded. The mutation found in WFS2 patients is a G to C base-pair transversion in pre-mRNA CISD2 that causes a splicing error, resulting in removal of the second exon and introduction of a premature stop codon, which eliminates 75% of the protein transcript (Fig. 1).¹ Indeed, the region binding the 2Fe-2S cluster is eliminated completely. Although initially healthy, patients with WFS2 experience a decreased life expectancy, early onset diabetes

*Corresponding authors. E-mail addresses: pajennings@ucsd.edu; mpaddock@ucsd.edu.

Abbreviations used: ER, endoplasmic reticulum; MAD, multiwavelength anomalous dispersion; OMM, outer mitochondrial membrane; SSRL, Stanford Synchrotron Radiation Lightsource.

[†] Also known as ERIS, CDGSH2.

[‡] Previous symbol ZCD2.

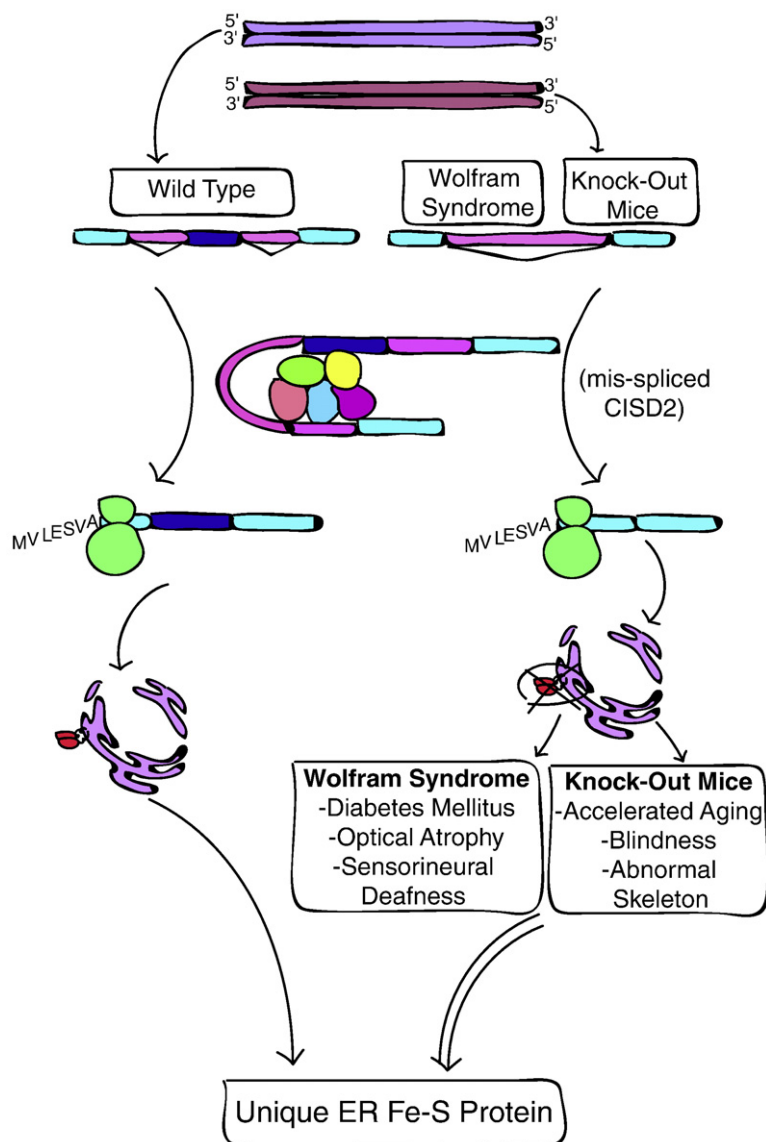


Fig. 1. Elimination of functional Miner1 protein leads to multiple symptoms in both human and mice models. C_{ISD}2, shown at the top, codes for an endoplasmic reticulum (ER) protein Miner1 (left-hand side). Amr *et al.* showed recently that Wolfram Syndrome 2 is attributed to a single base pair conversion in the C_{ISD}2 gene.¹ This mutation causes a splicing error that completely eliminates exon2 and creates a premature stop codon in exon 3 (right-hand side). For these reasons, 75% of the protein sequence is not translated,¹ and no Miner1 is properly assembled in the ER (lower part of right-hand side). The absence of this protein causes a wide range of symptoms in WFS2 patients, including diabetes mellitus and optical atrophy.¹ In an independent study, C_{ISD}2 knockout mice were constructed with a coding error that causes incorrect splicing, resulting in an inoperative gene.² Knock-out mice are also symptomatic, with similar signs of early aging and optical atrophy.²

mellitus, optical atrophy, sensorineural deafness, and a significant bleeding tendency.¹ Studies of structure and function of Miner1 are expected to provide critical information on the fundamental cause of the disease and reasons for the decrease in life expectancy.

C_{ISD}2 is on chromosome 4, a genetic locus associated with longevity. Investigations focused on the longevity locus where researchers disrupted C_{ISD}2 in mice found that the elimination of Miner1 resulted in decreased life expectancy and reduced general health.² These knockout mice show accelerated aging, blindness, an abnormal skeleton, and muscle atrophy,² effects that are very similar to those described in WFS2 patients. The mouse ortholog is 96% identical with the human Miner1 and is highly conserved (94–100%) in other mammals (Supplementary Data Fig. S1). Obtaining the Miner1 protein structure provides a basis for understanding the functional consequences of mutations in human and animal studies.

Miner1 belongs to a newly discovered family, which includes the 2Fe-2S-containing outer mitochondrial membrane (OMM) protein mitoNEET.^{3,4} In contrast, Miner1 localizes to the ER.¹ It contains an atypical ER localization sequence, an N-terminal transmembrane domain, and a CDGSH 2Fe-2S domain. To facilitate yields and structural studies, we focused on the soluble domain of the protein and made a point mutation at the only non-conserved free cysteine (Supplementary Data Fig. S1). In this work, we show that the Cys mutation does not affect the properties and report the crystal structure of the soluble region of Miner1 (C92S) solved at 2.1 Å resolution using Fe-MAD phasing.⁵ The structure is homodimeric with a scaffold similar to that of the OMM protein mitoNEET, but has a distinct surface topology and differences in the charge distribution. We report and compare redox and stability measurements as functions of pH for both Miner1 and its paralog mitoNEET.⁶

Results

Isolation and UV-visible spectroscopy of the ER protein Miner1

In an effort to understand the properties of this protein, we produced a soluble form of recombinant human Miner1 that corresponds to amino acids 57–135 (lacking the amino-terminal targeting and transmembrane sequences). The protein was fused to a cleavable His tag to facilitate purification. As a result, the construct includes an additional four amino acids (GSHM) at the N-terminus. Early attempts at purification were hindered by protein instability and aggregation. Although the use of reducing agent decreased aggregation, yields remained insufficient for structural studies. Therefore, we replaced the one free non-conserved cysteine (Supplementary Data Fig. S1) with the isosteric serine (C92S). The resultant mutant protein, Miner1 (C92S), has the same optical signature of the native Miner1 (Fig. 2). Furthermore, the construct had the desirable effects of improved yields of purified protein and a decreased tendency to aggregate. Since the point mutation does not change the spectra of Miner1, we refer to Miner1(C92S) simply as Miner1.

The overall fold of Miner1

The isolated purified recombinant protein showed CD spectra (Supplementary Data Fig. S2) indicative of a well-folded protein with a chiral center. The protein was amenable to crystallization. X-ray diffraction intensities were collected at Stanford Synchrotron Radiation Laboratory (SSRL) BL7-1 and

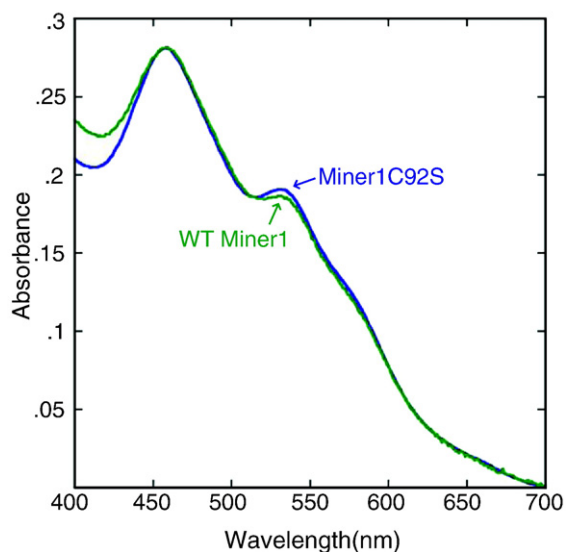


Fig. 2. Miner1 (C92S) has essentially the same UV-visible spectrum as WT Miner1. Both Miner1 (green) and Miner1 (C92S) (blue) show the same 2Fe-2S absorbance peaks at 460 nm and 530 nm. Thus, the C92S point mutation does not affect the Miner1 optical signature significantly.

BL9-2 to 2.1 Å (Table 1). Miner1 crystallized in the orthorhombic space group $P2_12_12_1$ with unit cell parameters $a=49.90$ Å, $b=48.58$ Å, $c=74.10$ Å, $\alpha=\beta=\gamma=90^\circ$ (Table 1). The Matthews coefficient (V_m) of the crystal was $2.0 \text{ \AA}^3/\text{Da}$ with an estimated solvent content of 37% (v/v).

Experimental phases for model building were determined with Fe-MAD.⁵ The model was refined using 2.1 Å data to an R -factor of 17.0% ($R_{\text{free}}=21.6\%$). The high quality of the electron density is shown in Fig. 3a. The refined model reveals a parallel homodimeric structure that includes the cytoplasmic fragment of each protomer from Asp68 to Glu134 on protomer A and to Val135 on protomer B (Fig. 3a). A total of 15 amino acids at the N-termini are disordered and not resolved in the electron density. The homodimer is tightly packed with

Table 1. Summary of crystal parameters, data collection, and refinement statistics for Miner1

Space group	$P2_12_12_1$		
Unit cell parameters			
a (Å)	49.90		
b (Å)	48.58		
c (Å)	74.10		
$\alpha=\beta=\gamma$ (°)	90		
A. Data collection			
	λ_1 FeMAD	λ_2 FeMAD	λ_3 FeMAD
Wavelength (Å)	1.7418	1.3624	1.7372
Resolution range (Å)	40.89–2.25	48.56–2.10	48.56–2.25
No. observations	197,570	244,886	197,223
	(28,295)	(36,669)	(28,261)
No. unique reflections	7347 (1025)	9047 (1288)	7349 (1024)
Completeness (%)	98.9 (97.6)	99.4 (98.7)	98.9 (97.5)
Mean $I/\sigma(I)$	23.2 (6.40)	24.9 (10.8)	23.8 (7.3)
R_{symm} on I (%)	12.1 (89.5)	10.9 (52.8)	11.7 (79.2)
B. Model and refinement statistics			
Data set used	λ_2		
Cutoff criterion	$ F > 0$		
Resolution range (Å)	37.1–2.10		
No. reflections (total)	9013 ^a		
No reflections (test)	450		
Completeness (% total)	99.2		
Mean $I/\sigma(I)$	17.6 (10.8)		
R_{symm} on I (%)	10.3 (52.8)		
R_{cryst}	17.0		
R_{free}	21.6		
Stereochemical parameters			
Restraints			
(RMS observed)			
Bond angles (°)	1.86		
Bond lengths (Å)	0.013		
Average isotropic B -value (Å ²)	27.58		
ESU based on R_{free} (Å)	0.164		

ESU, estimated overall coordinate error. $R_{\text{symm}} = \sum |I_i - \langle I \rangle| / \sum I_i$, where I_i is the scaled intensity of the i th measurement and $\langle I \rangle$ is the mean intensity for that reflection.

$R_{\text{cryst}} = \sum |F_{\text{obs}}| - |F_{\text{calc}}| / \sum |F_{\text{obs}}|$, where F_{calc} and F_{obs} are the calculated and observed structure factor amplitudes, respectively. $R_{\text{free}} = R_{\text{cryst}}$ for 5.0% of the total reflections chosen at random and omitted from the refinement. Values in parentheses are for the highest-resolution shell.

^a Typically, the number of unique reflections used in refinement is less than the total number that were integrated and scaled. Reflections are excluded due to systematic absences, negative intensities, and rounding errors in the resolution limits and cell parameters.

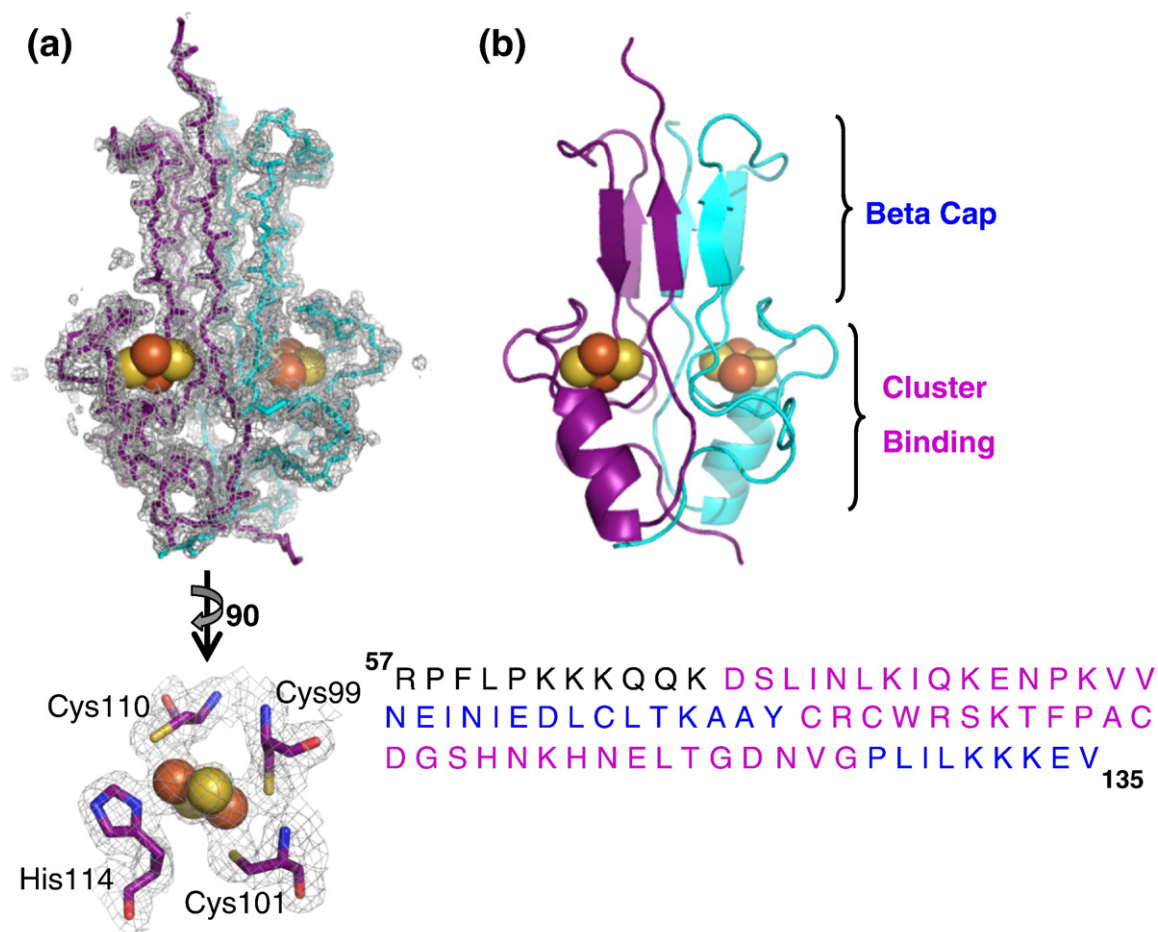


Fig. 3. Structural organization and domain topology of dimeric Miner1. (a) The backbone tracing of homodimeric Miner1 (upper). Protomers are colored purple and cyan together with the observed $2F_o - F_c$ electron density (gray) map contoured at 1.5σ . A 2Fe-2S cluster is present in each protomer (Fe, red spheres; S, yellow). The two protomers are related by a dyad axis along the vertical direction in the plane of the paper (see arrow). Lower: An expanded view of one 2Fe-2S cluster (rotated $\sim 90^\circ$ counterclockwise along the dyad axis) showing the cluster and iron ligands (O, red; N, blue; C, green) and the corresponding observed $2F_o - F_c$ electron density (gray) map contoured at 2.0σ . The amino acid ligands are indicated. Rendered with PyMol (<http://pymol.sourceforge.net/>). (b) Ribbon diagram highlighting the two domains and protomer interactions within the Miner1 homodimer: a six-stranded β sandwich forms an intertwined β cap and a larger cluster-binding domain carries two 2Fe-2S clusters (one per protomer). Below is the amino acid sequence of the construct. Coded segments contributing to each domain are highlighted on the primary sequence with blue for the β cap and magenta for the cluster-binding domains. The 2Fe-2S binding cradle is located sequentially between two parts of the β cap domains.

1800 \AA^2 of buried surface area at the interface, as calculated using PISA.⁷ Model validation using the MOLPROBITY⁸ structure validation tool indicates that 97% of the amino acid residues are in the favored region of Φ/Ψ space.

Miner1 is folded into two spatially distinct sub-regions: a β -rich or β -cap domain and a helical 2Fe-2S binding or cluster binding domain (Fig. 3b). The β -rich domain contains a strand swap from opposite ends of the primary sequence to form the β -cap structure. This domain contains 28 residues within β strands with two antiparallel strands coming from one protomer and the third parallel coming from the other (Fig. 3b). These two strand-swapped sheets pack together to form the β -cap sandwich domain and form the narrowest part (~ 15 \AA across) of the structure (Fig. 3b). The struc-

ture confirms the presence of two 2Fe-2S clusters expected from the optical spectrum (Fig. 2). These clusters are separated by approximately 16 \AA (center-to-center) within the larger helical cluster binding domain (~ 30 \AA across) (Fig. 3b). A structural similarity search using the DALI server⁹ revealed that this fold shows significant similarity only to the recently determined new structural NEET fold of mitoNEET.^{6,10,11} This is the first example of another protein that shares the NEET fold.

Structure of the 2Fe-2S clusters

The cluster binding domain consists of the sequences Asp68–Val83 and Cys99–Gly126 on each protomer (Fig. 3b). Each 2Fe-2S cluster is cradled by a relatively short polypeptide chain, Cys99–Gly112.

This segment contains the three coordinating Cys ligands (Cys99, Cys101, Cys110) and the single coordinating His ligand (His114). His114 is near the N-terminus of the α -helix within the cluster-binding domain (Ala113–Thr121) (Fig. 3).

Cys110 and His114, which coordinate the outermost Fe, are solvent-accessible, as illustrated in Fig. 4 by their semitransparent surfaces. In contrast, Cys99 and Cys101, which coordinate the innermost Fe, are buried within the structure (Fig. 4). Located sequentially between the innermost Cys ligands is Arg100. It forms interprotomer interactions near the 2Fe-2S clusters. Its guanidinium group forms a direct interprotomer hydrogen bond with the amide side chain of Asn84 of the other protomer. In addition, Arg100 interacts with the backbone oxygens of Cys99 and Pro108 of the other protomer *via* an internal water molecule (Fig. 4) locking Pro108 into a *cis* conformation.

The proton-coupled redox potential of the 2Fe-2S clusters of Miner1 and its paralog mitoNEET

A property of Miner1 that relates to possible redox activity is its redox potential E_m . The E_m values of both Miner1 and mitoNEET, i.e. $[2\text{Fe-2S}]^{2+}/[2\text{Fe-2S}]^+$,

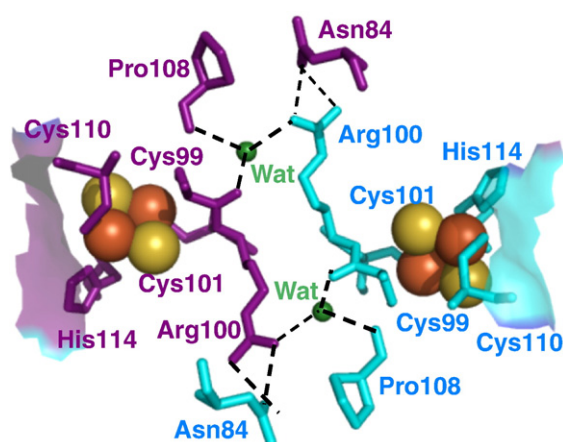


Fig. 4. The 2Fe-2S cluster binding cradle. View of the 2Fe-2S cluster (Fe as brown and S as yellow spheres) from a perspective rotated $\sim 90^\circ$ along an axis perpendicular to the dyad axis from that shown for the cluster binding site in Fig. 3a. The amino acids belonging to the individual protomers are shown in purple and cyan, respectively. The two 2Fe-2S cradles are related to each other *via* a 180° rotation along the dyad symmetry axis of the dimer located approximately perpendicular to the page. Cys110 and His114 bind the outermost Fe, while the innermost Fe is bound by Cys99 and Cys101 (as indicated). The solvent-accessible His114 is located at the end of the prominent α helix in the cluster binding domain (Fig. 3). Two additional residues, Arg100 and Asn84, form an interprotomer bifurcated hydrogen bond within the interior of the protein dimer. Each Arg100 also forms a potential hydrogen bond with one of two internal water molecules (shown as green spheres and labeled as Wat) that form additional interprotomer hydrogen bonds with the backbone oxygen atoms of Cys99 and Pro108.

were measured spectroscopically by the change in visible absorbance that occurs upon reduction (Supplementary Data Fig. S3). The fraction oxidized was plotted as a function of the measured ambient redox potential (Supplementary Data Fig. S3) and fit by the Nernst equation as described,¹² yielding an E_m of ~ 0 mV (± 10 mV) at pH 7.5 for both Miner1 and mitoNEET.

In order to determine the influence of charges and titratable groups on E_m , the pH dependence was measured. The E_m values of both Miner1 and mitoNEET are pH-dependent from pH 7.5 to 10.0 decreasing 50 mV per pH unit (Fig. 5a). The observed dependence shows the reduction is proton-coupled, which is often of functional relevance.¹³

Drastic difference in the half-life of the 2Fe-2S clusters of Miner1 and mitoNEET

Investigations of the release of the 2Fe-2S clusters can provide information on key interactions between the clusters and the protein. The half-life of the 2Fe-2S clusters was determined from monitoring the cluster absorbance from 320 nm to 600 nm as a function of time at 35°C (Supplementary Data Fig. S4). A half-life of 700 min (pH 7.1) was determined from the observed signal change as a function of time. Surprisingly, given the similar fold, Miner1 was 10-fold less stable than mitoNEET¹⁴ (Fig. 5b). In contrast, Miner1 was more stable at pH 5.3 (Supplementary Data Fig. S4). In addition, the decay is more non-exponential, suggesting a more complex unfolding energy landscape.¹⁵ To further explore differences, we performed a more detailed investigation of the stability as a function of pH.

Investigation of the stability as a function of pH provides additional information on interactions between titrating (charged) residues and the cluster. In contrast to mitoNEET, the lifetime for Miner1 varies by only ~ 5 -fold from pH 5.3 to 7.1 compared to ~ 300 -fold for mitoNEET (Fig. 5b). Thus, the release of the 2Fe-2S clusters of Miner1 is orders of magnitude less sensitive to pH as that of mitoNEET.

Prominent differences in the charge distribution of Miner1 and mitoNEET and in the packing of the β -cap domain

The two proteins display prominent differences in the distribution of charges. Overall, Miner1 has both fewer charged (Asp and Lys) and His residues (Fig. 6b). The homologous sites of polar Asn87 and apolar Leu93 and Leu120 in Miner1 are acidic (Asp61, Asp67 and Asp93) in mitoNEET. Other differences include: (i) polar Thr106 in Miner1 replaced with a basic Lys79 in mitoNEET; (ii) acidic Glu85 by neutral Ala59; and (iii) Lys74 and Asn84 by His48 and His58, respectively. These changes result in a more positively charged soluble domain for Miner1.

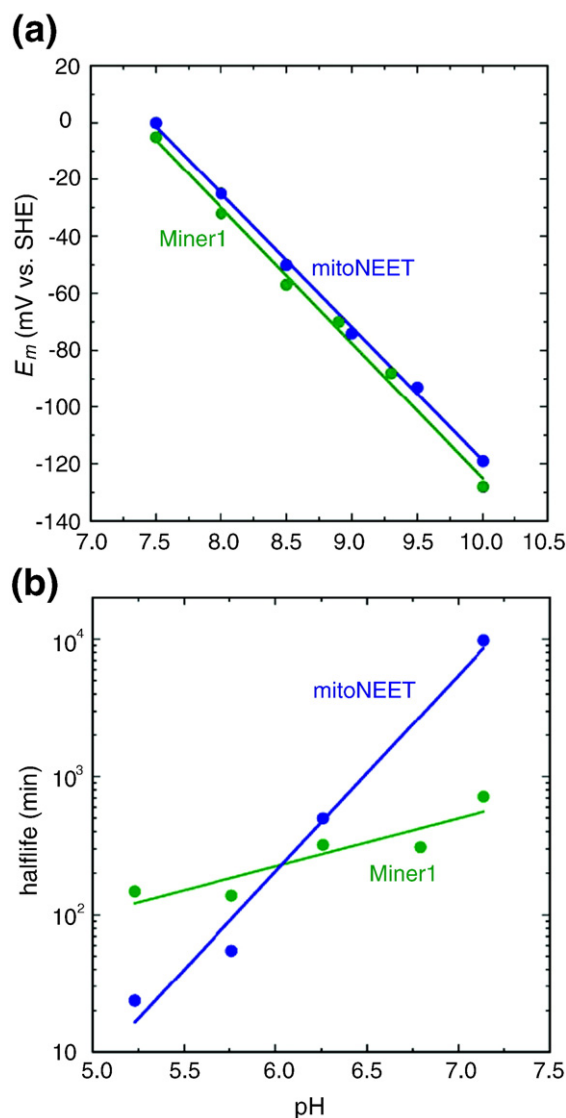


Fig. 5. Redox potential and stability of the 2Fe-2S clusters of Miner1 and mitoNEET. (a) pH-dependence of the redox potentials (E_m) of Miner1 and mitoNEET. Both display pH-dependent E_m values from pH 7.5 to 10.0 that decrease by 50 mV per pH unit, indicating that the reduction is proton-coupled. (b) pH-dependence of the 2Fe-2S cluster stabilities of Miner1 and mitoNEET. The half-life for Miner1 is orders of magnitude less pH-dependent varying by only ~ 5 -fold from pH 5.3 to 7.1 compared to the ~ 300 -fold change for mitoNEET.

The similarities and differences in the properties of Miner1 and mitoNEET are evident when the two structures are superimposed (Fig. 6). Miner1 is the second known member of the family first established by the determination of the mitoNEET structure (Fig. 6).^{6,10,11} The cluster-binding domains of Miner1 and mitoNEET share the same Cys₃-His 2Fe-2S coordination and are structurally the same within uncertainty (rmsd ~ 0.3 ; PDB ID 2QH7).⁶

However, superposition of the dimeric structures reveals significant differences in the outermost strands. The backbone rmsd of the β -cap domain is

~ 1.1 Å, ~ 4 -fold greater than that of the cluster binding domain (Fig. 6a). These differences result in a more open V shape appearance in the β -cap of Miner1. As an additional test of the significance of this apparent difference, we superimposed the protomer structures of Miner1 and mitoNEET (Fig. 7a). Strikingly, the central strand along with the cluster binding domain of the protomers are superimposable. However, the outer strands (circled) are shifted with respect to one another. Interestingly, Miner1 has an amino acid insertion at the top of the β -cap domain (Thr 94; Fig. 7, highlighted) that appears to act as a spacer extending the distance between the central and the outer strand. In addition, several key variations in aromatic residues (Phe60/Ile86 and Phe82/Ala109) create differences in side chain orientation and appear to affect the position of Tyr71/Tyr98, with a relative displacement of 2.2 Å.

Discussion

We report here the crystal structure determined to 2.1 Å resolution of the ER protein Miner1. We show that, contrary to its original annotation, it contains redox-active 2Fe-2S clusters with an $E_m \sim 0$ mV at pH 7.5. Miner1 is a member of the novel 2Fe-2S CDGSH protein family and the first FeS protein localized to the ER. Mis-splicing of the mRNA that codifies this protein is causative in the genetic disease Wolfram Syndrome 2 (WFS2). FeS proteins participate in many types of biochemical reactions, the most predominantly characterized are oxidation-reduction reactions, but they also participate in Fe-S cluster assembly and gene expression regulation.^{16–19} Although not yet determined *in vivo*, Miner1 has biophysical properties necessary to participate in the functions that have a vital role in homeostasis required for proper health and longevity. The importance of Miner1 in cellular health is evidenced in the deleterious effects of its absence in WFS2 and knockout mice.^{1,2} The potential role this protein plays in human health and defense against environmental stresses is suggested by the fact that patients with WFS2 can live to 15 years before becoming symptomatic.

Miner1 is the first 2Fe-2S protein found in the ER

Miner1 was identified as one of a small family of proteins that share the CDGSH sequence domain.⁴ On the basis of strong perinuclear staining and its localization to a lacy network in V5 epitope studies performed in transiently expressed COS-7 cells, Wiley *et al.* suggested that Miner1 localizes to the ER.⁴ Amr *et al.* subsequently confirmed this suggestion in mouse P19 cells in which N-FLAG tagged Miner1 colocalized with calnexin, a known ER marker.¹ Taken together with our structural studies (Fig. 3), Miner1 is to our knowledge the first 2Fe-2S-containing protein localized to the ER membrane.

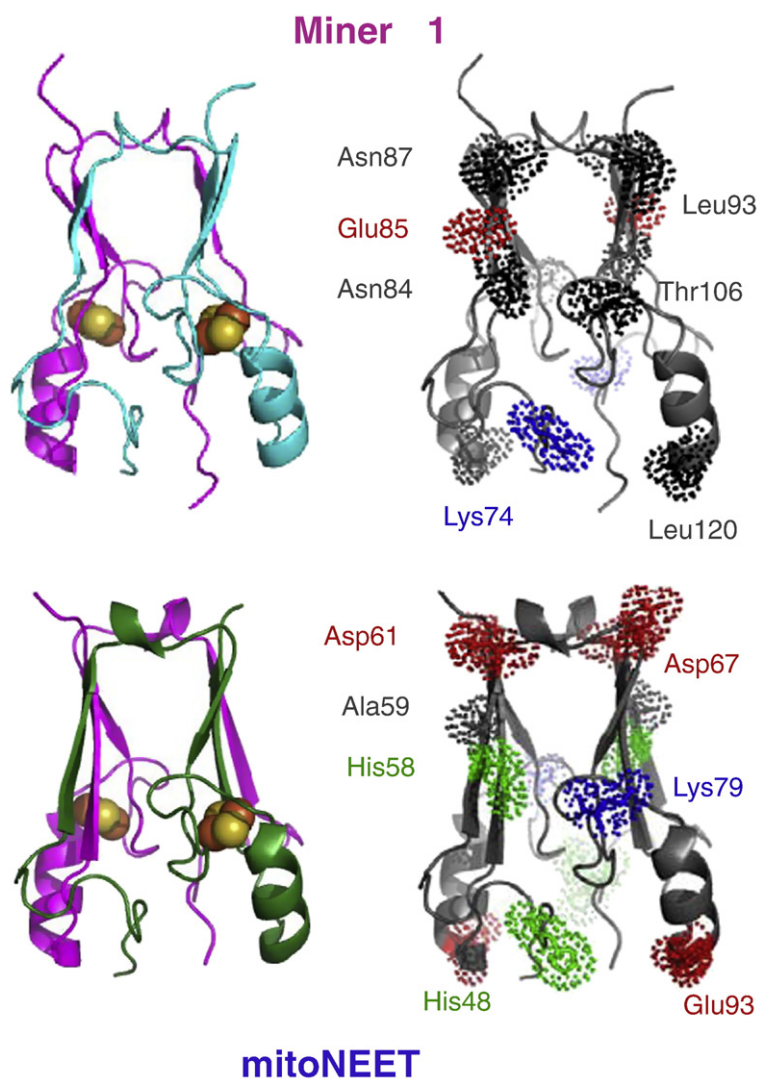


Fig. 6. Differences in the backbone and charge distributions of Miner1 and related mitoNEET structures. (left) Ribbon diagrams of Miner1 and mitoNEET⁶ from a perspective rotated 90° along the dyad axis from that in Fig. 3b. The two proteins share a similar fold, previously termed the NEET fold. The cluster binding domains are nearly superimposable. In contrast, there are differences greater than the uncertainty in the β cap domains, with Miner1 appearing more open near the top and forming more of a V shape. (right) The sites where amino acid differences between Miner1 and mitoNEET result in either a change in a charged or a titratable group are highlighted. In most cases, the neutral residues of Miner1 are replaced with acidic groups or His in mitoNEET, resulting in a more positively charged soluble domain for Miner1. Ribbon backbone, gray; neutral residues, black; negative residues, red; positive residues, blue; and His, green. For clarity, sites of changes are labeled on only one of the protomers.

Proton-coupled redox activity of Miner1

One of the best characterized functions of FeS proteins is their role in redox reactions. A primary property that relates to this function is the redox potential E_m . The E_m of Miner1 and mitoNEET were measured *via* equilibrium titration to be essentially the same at ~ 0 mV at pH 7.5. The similarity of their E_m values is expected as both Miner1 and mitoNEET have nearly superimposable structures of the cluster binding domains that include the rare Cys₃-His coordination. The E_m values vary by -50 mV/pH unit indicating that the reductions are proton-coupled (Fig. 5a). Since both Miner1 and mitoNEET display the same behavior, the site of protonation is also likely the same. Given the magnitude of the change in redox potential (>150 meV), the protonation site must be located near the 2Fe-2S cluster. In addition to the inorganic sulfide of the cluster, the 2Fe-2S clusters share ligation by Cys110 and His114, and interact with the nearby Asp111 and Ser104. Further localization of the proton requires additional investigation.

The most common redox-active motifs for 2Fe-2S proteins are ferredoxin-like, whose clusters are coordinated by four Cys, and Rieske-like, whose clusters are coordinated by two Cys and two His. The Fd-like proteins tend to have negative E_m (~ -300 mV) and the Rieske-like positive E_m ($\sim +300$ mV), although some can be in the same range as Miner1.¹⁷ Miner1 and mitoNEET have redox potentials similar to those of known electron transfer species such as cytochrome *b* and quinones.^{20,21} Thus, their potentials are within the physiological range consistent with Miner1 and mitoNEET participating in electron transfer or oxidation/reduction reactions in the cell.

Different pH sensitivity of the 2Fe-2S clusters of Miner1 and mitoNEET

Another known functional role for FeS proteins is cluster assembly and transfer.¹⁹ The Miner1 family shares the unusual Cys₃-His coordination with only one other known protein structure—that of an IscU D38A mutant from a hyperthermophilic bacteria,²² a protein that participates in cluster assembly. In

order for this function to be plausible for Miner1, the Fe-S cluster must be easily transferable or labile. The measured lifetime of the 2Fe-2S clusters of Miner1 was ~10-fold shorter at pH 7.1 than that of mitoNEET.⁴ This lability is accelerated by orders of magnitude in cellular extracts (data not shown), suggesting a possible role of Miner1 in FeS cluster assembly and/or transfer.

Surprisingly, given the highly similar structure of Miner1 and mitoNEET, the lability of the two proteins displayed drastically different pH dependence. Whereas the lability of Miner1 varied by only ~5-fold from pH 5.3 to 7.1, mitoNEET varied ~300-fold over the same pH range (Fig. 5). This difference in the lability is likely due to differences in the charged or titratable groups of the proteins. A site-specific comparison revealed seven differences between the proteins (Fig. 6)—Lys74, Asn84, Glu85, Asn87, Leu93, Thr106, and Leu120. One or more of these changes is likely responsible for the altered pH sensitivity.

Miner1, ER function and health and disease

Miner1 is targeted to the ER membrane,^{1,4} the organelle in which lipid synthesis, protein folding and protein maturation take place. A number of post-translational modifications are performed here, including lipidation, hydroxylation, glycosylation, methionine and cysteine oxidation.^{23,24} The ER participates in quality control by facilitating the recognition and targeting of aberrant proteins for degradation.²⁵ When its capacity is exceeded, a signaling network called the unfolded protein response is activated.²⁴ The redox ability of Miner1 could allow it to participate in protein modification and possible ER stress responses.

Recent studies on the tethering of the ER and mitochondria *via* the protein mitofusin indicate that a direct interaction between the organelles is essential for Ca²⁺ transfer and cellular function.^{26,27} Increasing evidence also links altered communication between the ER and mitochondria to apoptosis and disease.^{28–30} Mitochondrial-ER crosstalk is implicated in type 2 diabetes.^{23,31–34} Interestingly, Miner1 is situated on the surface of the ER and mitoNEET is on the surface of the OMM. The similarity of their E_m values indicates that they would respond to similar redox stimuli and could possibly communicate through electron transfer, thus providing a means of ER-mitochondrial crosstalk.

Proper biological function of Miner1 is necessary for cellular health, as the absence of Miner1 has deleterious effects, such as WFS2¹ or decreased longevity (Fig. 1).² The similarities of Miner1 with its paralog mitoNEET also strengthen the link between proper function of this novel family of 2Fe-2S proteins and general health. Thus, further investigation of the interplay between the functional and biophysical properties of this family is anticipated to advance our understanding of these complex mechanisms involved in health and metabolic disease.

Materials and Methods

Expression and purification

The soluble domain of miner1 (residues 57–135; cDNA purchased from Open Biosystems) was amplified by PCR and subcloned into the bacterial expression vector pET28a(+) (Novagen) containing an N-terminal, thrombin cleavable His tag. The C92S mutation was made by site-directed mutagenesis using PCR. This plasmid was transformed into BL21-RIL(DE3) (Stratagene) and grown as described.⁶ Harvested cells were suspended in binding buffer (20 mM Tris-HCl pH 7.9, 5 mM imidazole, 500 mM NaCl). After centrifugation, the lysate was added to Ni-NTA resin, which was washed with 10 column volumes of wash buffer (20 mM Tris-HCl pH 7.9, 30 mM imidazole, 500 mM NaCl), equilibrated in thrombin cleavage buffer (25 mM Tris-HCl pH 8.0, 100 mM NaCl, 2.5 mM CaCl₂), and cleaved upon addition of thrombin at room temperature for 16–24 h. Miner1 was eluted with wash buffer and further purified by size-exclusion chromatography (S-200 GE Healthcare) in 25 mM Tris-HCl pH 8.0, 100 mM NaCl. For crystallographic experiments, the protein was further purified by cation-exchange chromatography (HiTrap, GE Healthcare) as described.⁶

Optical spectroscopy and stability measurements

All UV-visible absorption spectra were measured from the near-UV to the near-IR (250 – 700 nm) at 35 °C with a Cary50 spectrometer (Varian Inc, Palo Alto CA) (10–20 μM protein in 25 mM Tris-HCl pH 8.0, 100 mM NaCl).

The stabilities of the 2Fe-2S clusters were determined from monitoring their characteristic absorbance at 460 nm as a function of time following dilution of the protein into the assay buffer (~20 μM protein in 100 mM buffer at 35 °C) (Supplementary Data Fig. S3). The following buffers were used at the pH indicated: Tris-HCl at pH 7.1 and 6.8, and bis-Tris-HCl at pH 6.3, 5.8 and 5.3. Both the buffer and the protein were filtered before the start of the measurement and a layer of paraffin oil was placed over the solution to minimize evaporation. The half-life corresponding to 50% decay was determined at each pH value.

Redox measurements

The reduction state was determined by monitoring the absorbance near 460 nm with 100 μM protein in 25 mM Tris-HCl pH 7.5, 100 mM NaCl at 25 °C under positive argon pressure using a quartz cuvette with a side-arm (Airgas-West, San Diego CA) (Supplementary Data Fig. S4). A Ag/AgCl dual reference and working electrode (Microelectrodes Inc, Bedford NH) was used to measure the ambient redox potential. Its calibration was checked using quinhydrone at pH 4.0 and pH 7.0 as recommended. Then 50 mM pH-buffered dithionite (Fisher Scientific, Pittsburgh PA) was added *via* a Hamilton syringe to adjust the redox potential; and 50 μM ubiquinone (Sigma-Aldrich), 50 μM duroquinone (Sigma-Aldrich), 100 μM menadione (Sigma-Aldrich), and 100 μM naphthaquinone (Sigma-Aldrich) were added to ensure efficient electron transfer between the solution components and the electrode. Origin 6.1 (OriginLab Corporation) was used to determine the

midpoint/redox potential (E_m) from a fit of the fraction oxidized to the Nernst equation:

$$A = A_{\text{ox}} \{1 + 10^{[(E_m - E)(n/59.1 \text{ mV})]}\} + A_{\text{red}}$$

where A_{ox} is the absorbance of the fully oxidized sample, E_m is the midpoint potential in mV, E is the measured cell potential in mV, n is the number of electrons being transferred in the redox reaction, and A_{red} is the lowest absorbance level corresponding to the fully reduced 2Fe-2S center in either native or mutant mitoNEET. Potentials were adjusted to SHE for presentation. Samples were tested for their ability to re-oxidize upon exposure to ambient oxygen.

Crystallization

Crystallization was achieved as described for mitoNEET.⁶ The final conditions were 100 mM Tris-HCl pH 8.0, 100 mM NaCl, and 15–20% (w/v) PEG 3000 in the protein well, equilibrating against 100 mM Tris-HCl pH 8.0 and 30–33% PEG 3000 in the reservoir. Crystals were frozen at 77 K after soaking for 1 min in 100 mM Tris-HCl pH 8.0, 40% PEG3000 and sent frozen (77 K) to SSRL in an SSRL-supplied cassette system for X-ray data collection and analysis.

X-ray data collection and structural determination

Frozen crystals were screened using the Stanford Automated Mounter³⁵ operated by Blu-Ice.³⁶ The data were recorded using a Rayonix MX-325 CCD detector at BL9-2 and an ADSC Q315R CCD detector at BL7-1. Data were processed with XDS.³⁷ The structure of Miner1 was determined by MAD phasing.^{5,38} Data reduction and primary phasing at a resolution of 2.1 Å were accomplished as described.⁶

Protein Data Bank accession numbers

The atomic coordinates have been deposited in the Protein Data Bank: PDB ID code 3FNV; RCSB ID code rcsb050821.

Acknowledgements

This work was supported by grants from the NIH grants GM 41637 (to M. Okamura and M.L.P.), and GM54038 and DK54441 (to P.A.J.). Students were supported by HEME and CMG training grants. R. N. thanks the Zevi Hermann Shapira Foundation for supporting the collaborative USA-Israeli efforts. We thank Christopher L. Rife at the Joint Center for Structural Genomics (JCSG) for providing an automated programming script for coordinate validation, Mitch Miller at SSRL and JCSG for helpful discussions on the data collection and processing, and Mel Okamura and JCSG for helpful discussions and support. Parts of this research were carried out at the Stanford Synchrotron Radiation Laboratory, a national user facility operated by Stanford University on behalf of the U.S. Department of Energy, Office of Basic Energy

Sciences. The SSRL Structural Molecular Biology Program is supported by the Department of Energy, Office of Biological and Environmental Research, and by the National Institutes of Health, National Center for Research Resources, Biomedical Technology Program, and the National Institute of General Medical Sciences.

Supplementary Data

Supplementary data associated with this article can be found, in the online version, at doi:10.1016/j.jmb.2009.06.079

References

1. Amr, S., Heisey, C., Zhang, M., Xia, X. J., Shows, K. H., Ajlouni, K. *et al.* (2007). A homozygous mutation in a novel zinc-finger protein, ERIS, is responsible for Wolfram syndrome 2. *Am. J. Hum. Genet.* **81**, 673–683.
2. Tsai, T., Chen, Y., Tsai, S. & Chen, Y. (2008). Cisd2-knockout mice and uses thereof. In *United States Patent Trademark Office*, p. 19, National Yang-Ming University, Taipei City (TW), National Health Research Institutes, Miaoli County (TW), USA.
3. Colca, J. R., McDonald, W. G., Waldon, D. J., Leone, J. W., Lull, J. M., Bannow, C. A. *et al.* (2004). Identification of a novel mitochondrial protein ("mitoNEET") cross-linked specifically by a thiazolidinedione photoprobe. *Am. J. Physiol. Endocrinol. Metab.* **286**, E252–E260.
4. Wiley, S. E., Murphy, A. N., Ross, S. A., van der Geer, P. & Dixon, J. E. (2007). MitoNEET is an iron-containing outer mitochondrial membrane protein that regulates oxidative capacity. *Proc. Natl Acad. Sci. USA*, **104**, 5318–5323.
5. Pahler, A., Smith, J. L. & Hendrickson, W. A. (1990). A probability representation for phase information from multiwavelength anomalous dispersion. *Acta Crystallogr. A*, **46**, 537–540.
6. Paddock, M. L., Wiley, S. E., Axelrod, H. L., Cohen, A. E., Roy, M., Abresch, E. C. *et al.* (2007). MitoNEET is a uniquely folded 2Fe-2S outer mitochondrial membrane protein stabilized by pioglitazone. *Proc. Natl Acad. Sci. USA*, **104**, 14342–14347.
7. Krissinel, E. & Henrick, K. (2007). Inference of macromolecular assemblies from crystalline state. *J. Mol. Biol.* **372**, 774–797.
8. Lovell, S. C., Davis, I. W., Adrendall, W. B., de Bakker, P. I. W., Word, J. M., Prisant, M. G. *et al.* (2003). Structure validation by C alpha geometry: phi, psi and C beta deviation. *Proteins: Struct. Funct. Genet.* **50**, 437–450.
9. Holm, L. & Sander, C. (1995). Dali - a network tool for protein-structure comparison. *Trends Biochem. Sci.* **20**, 478–480.
10. Lin, J. Z., Zhou, T., Ye, K. Q. & Wang, J. F. (2007). Crystal structure of human mitoNEET reveals distinct groups of iron-sulfur proteins. *Proc. Natl Acad. Sci. USA*, **104**, 14640–14645.
11. Hou, X. W., Liu, R. J., Ross, S., Smart, E. J., Zhu, H. N. & Gong, W. M. (2007). Crystallographic studies of human MitoNEET. *J. Biol. Chem.* **282**, 33242–33246.
12. Dutton, P. L. (1978). Redox potentiometry: determination of midpoint potentials of oxidation-reduction components of biological electron transfer systems. *Methods Enzymol.* **54**, 411–435.

13. Chang, C. J., Chang, M. C., Damrauer, N. H. & Nocera, D. G. (2004). Proton-coupled electron transfer: a unifying mechanism for biological charge transport, amino acid radical initiation and propagation, and bond making/breaking reactions of water and oxygen. *Biochim. Biophys. Acta*, **1655**, 13–28.
14. Wiley, S. E., Paddock, M. L., Abresch, E. C., Gross, L., van der Geer, P., Nechushtai, R. *et al.* (2007). The outer mitochondrial membrane protein mitoNEET contains a novel redox-active 2Fe-2S cluster. *J. Chem.* **282**, 23745–23749.
15. Onuchic, J. N., Kobayashi, C., Miyashita, O., Jennings, P. & Baldrige, K. K. (2006). Exploring biomolecular machines: energy landscape control of biological reactions. *Phil. Trans. Roy. Soc B*, **361**, 1439–1443.
16. Rees, D. C. & Howard, J. B. (2003). The interface between the biological and inorganic worlds: iron-sulfur metaloclusters. *Science*, **300**, 929–931.
17. Meyer, J. (2008). Iron-sulfur protein folds, iron-sulfur chemistry, and evolution. *J Biol. Inorg. Chem.* **13**, 157–170.
18. Bandyopadhyay, S., Chandramouli, K. & Johnson, M. K. (2008). Iron-sulfur cluster biosynthesis. *Biochem. Soc. Trans.* **36**, 1112–1119.
19. Lill, R. & Muhlenhoff, U. (2008). Maturation of iron-sulfur proteins in eukaryotes: mechanisms, connected processes, and diseases. *Annu. Rev. Biochem.* **77**, 669–700.
20. Rivera, M., Seetharaman, R., Girdhar, D., Wirtz, M., Zhang, X., Wang, X. & White, S. (1998). The reduction potential of cytochrome b5 is modulated by its exposed heme edge. *Biochemistry*, **37**, 1485–1494.
21. Berg, J., Tymoczko, J. & Stryer, L. (2003). *Biochemistry*, 5th edit., pp. 734–788, W. H. Freeman, New York.
22. Shimomura, Y., Wada, K., Fukuyama, K. & Takahashi, Y. (2008). The of [2Fe-2S] IscU: implications for its scaffolding during iron-sulfur cluster biosynthesis. *J. Mol. Biol.* **383**, 133–143.
23. Rajan, S. S., Srinivasan, V., Balasubramanyam, M. & Tatu, U. (2007). Endoplasmic reticulum (ER) stress & diabetes. *Indian J. Med. Res.* **125**, 411–424.
24. Schroder, M. & Kaufman, R. J. (2005). ER stress and the unfolded protein response. *Mutat. Res.* **569**, 29–63.
25. Hebert, D. N. & Molinari, M. (2007). In and out of the ER: Protein folding, quality control, degradation, and related human diseases. *Physiol. Rev.* **87**, 1377–1408.
26. Merkwirth, C. & Langer, T. (2008). Mitofusin 2 builds a bridge between ER and mitochondria. *Cell*, **135**, 1165–1167.
27. de Brito, O. M. & Scorrano, L. (2008). Mitofusin 2 tethers endoplasmic reticulum to mitochondria. *Nature*, **456**, 605–610.
28. Zhao, L. H. & Ackerman, S. L. (2006). Endoplasmic reticulum stress in health and disease. *Curr. Opin. Cell Biol.* **18**, 444–452.
29. Boya, P., Cohen, I., Zamzami, N., Vieira, H. L. A. & Kroemer, G. (2002). Endoplasmic reticulum stress-induced cell death requires mitochondrial membrane permeabilization. *Cell Death Differ.* **9**, 465–467.
30. Takuma, K., Yan, S. S. D., Stern, D. M. & Yamada, K. (2005). Mitochondrial dysfunction, endoplasmic reticulum stress, and apoptosis in Alzheimer's disease. *J. Pharmacol. Sci.* **97**, 312–316.
31. Hacki, J., Egger, L., Monney, L., Conus, S., Rosse, T., Fellay, I. & Borner, C. (2000). Apoptotic crosstalk between the endoplasmic reticulum and mitochondria controlled by Bcl-2. *Oncogene*, **19**, 2286–2295.
32. Ozcan, U., Cao, Q., Yilmaz, E., Lee, A. H., Iwakoshi, N. N., Ozdelen, E. *et al.* (2004). Endoplasmic reticulum stress links obesity, insulin action, and type 2 diabetes. *Science*, **306**, 457–461.
33. Nakatani, Y., Kaneto, H., Kawamori, D., Yoshiuchi, K., Hatazaki, M., Matsuoka, T. *et al.* (2005). Involvement of endoplasmic reticulum stress in insulin resistance and diabetes. *J. Biol. Chem.* **280**, 30648.
34. Marciniak, S. J. & Ron, D. (2006). Endoplasmic reticulum stress signaling in disease. *Physiol. Rev.* **86**, 1133–1149.
35. Cohen, A. E., Ellis, P. J., Miller, M. D., Deacon, A. M. & Phizackerley, R. P. (2002). An automated system to mount cryo-cooled protein crystals on a synchrotron beamline, using compact sample cassettes and a small-scale robot. *J. Appl. Crystallogr.* **35**, 720–726.
36. McPhillips, T. M., McPhillips, S. E., Chiu, H. J., Cohen, A. E., Deacon, A. M., Ellis, P. J. *et al.* (2002). Blu-Ice and the Distributed Control System: software for data acquisition and instrument control at macromolecular crystallography beamlines. *J. Synchrotron Radiat.* **9**, 401–406.
37. Kabsch, W. (1993). Automatic processing of rotation diffraction data from crystals of initially unknown symmetry and cell constants. *J. Appl. Crystallogr.* **26**, 795–800.
38. Terwilliger, T. C. & Berendzen, J. (1999). Automated MAD and MIR structure solution. *Acta Crystallogr. D*, **55**, 849–861.

Note added in proof: Since the work was submitted for publication, a Taiwanese consortium published an extensive paper on the characteristics of *cisd2* knockout mice (Chen, Y. F., Kao, C. H., Chen, Y. T., Wang, C. H., Wu, C. Y., Tsai, C. Y. *et al.* (2009). *Genes Dev.* **23**, 1183–1194). Furthermore, they showed that the knockout mice had a reduced electron transport activity of complex I-III, complex II-III and complex IV. They localized Miner1 to both the OMM and the ER with a 6:1 ratio. In our work, we present the structure of the protein that is key to their model for longevity and WFS2.